Urban heat island in the city of Brasilia: A multi-method analysis

Roberto Angeles-Vasquez[1], Julio Miguel Angeles-Suazo[2],
Carmencita Lavado-Meza[2], Jairo Edson Gutiérrez-Collao[2],
Pabel Mariano Meza-Mitma[2], Leonel de la Cruz-Cerron[3],
Jose Flores Rojas[4], Hugo Abi Karam[5], Nataly Angeles-Suazo[6*]

[1] Universidad Nacional del Centro del Perú, Huancayo, Junín, Perú
[2] Universidad Nacional Autónoma de Tayacaja Daniel Hernández Morillo, Pampas, Huancavelica, Perú
[3] Universidad Continental, Huancayo, Perú
[4] Instituto Geofisico del Perú, Huancayo, Perú
[5] Universidade Federal do Rio de Janeiro, Rio de Janeiro, Brazil
[6] Universidad Tecnológica del Perú, Huancayo, Junín, Perú
* Corresponding author's e-mail: nati2643@hotmail.com

ABSTRACT

Currently, cities are experiencing increased urbanization and population density, leading to an increase in natural areas covered by paved and built-up areas, with a very rapid rate of urban expansion, as in the case of the capital Brasilia, Brazil. This has led to changes in local climates, increasing land surface temperature (LST) and causing an effect known as the surface urban heat island (SUHI) directly related to natural vegetation and urban and rural areas – which has become a major challenge for societies around the world due to its implications for public health and the environment. In this regard, the objective was to compare the temporal variation (2001–2016) of the SUHI in the Metropolitan Region of Brasilia (MRG) with MODIS satellite images, using the quantile method and Streutker method. The results indicate a maximum daytime SUHI in January (3.08 °C) and minimum in July (1.51 °C); the nighttime SUHI had maximums in July (2.36 °C) and minimums in April (1.72 °C). The Quantile-Streutker correlation ≈ 0.10, highlighting the usefulness of the quantile method for cities with different maximum temperature centers on a non-Gaussian surface.

Keywords: urban heat island, urban areas, Streutker's method, quantiles method.

INTRODUCTION

In recent decades, cities have experienced a significant increase in urban temperature due to population growth caused by informal and formal urban development, which leads to changes in land use and increases in infrastructure and internal mobility needs, ultimately resulting in paved and built-up areas (Abdullah and Al-Alwan, 2019). While urbanization improves economic, social, and environmental aspects, it can raise serious questions about the sustainability and livability of metropolitan areas (Wu et al., 2024). Urban expansion causes changes in the Earth's surface, leading to variations in local climates and creating microclimates in urban areas, which are warmer than their natural or rural surroundings at specific times of day in mid-latitude locations (Angeles et al., 2024; Reyes and Aguiluz, 2023), This effect is known as the urban heat island (UHI) (Parece et al., 2016).

It should be noted that the UHI is the difference between the temperature of urban and rural areas, the nature of the contributing factors, and the urban fabric, while the surface urban heat island (SUHI) is the difference between the surface temperature (horizontal, vertical, inclined, and ground level) of solid urban and rural surfaces (Mirabi and Davies, 2022).

The Metropolitan Region of Brasília, known for being the third largest Brazilian metropolis in Brazil, has a population of 2,817,381 inhabitants according to the 2022 census, with an estimate for 2024 of 2,982,818 inhabitants and an urban area of 590.22 km^2 (Brazilian Institute of Geography and Statistics [IGBE], 2025). However, it had the highest population growth between 1960 and 2018, with a change in urban expansion planning policies between 2000 and 2016, increasing in size and moving away from a monocentric structure to gradually become polycentric (Costa and Lee, 2019), despite having been built with a completely different vision (known as the Pilot Plan), generating a physical transformation with respect to its expansion (Fraser, 2004). For example, mass migration led to urban expansion and increased requirements for technical infrastructure, water supply and disposal, nutrition, and energy (Banzhaf et al., 2009).

The progressive increase in urban density and urbanization reduces the amount of open natural spaces and vegetation cover, replacing them with buildings, roads, and concrete surfaces (Tawfeeq Najah et al., 2023), causing an increase in the SUHI phenomenon (Athukorala and Murayama, 2020) and an excessive rise in temperature (Gupta et al., 2020), as it increases the number of spaces that absorb heat and decrease cooling through evapotranspiration (Leonardo et al., 2025; Mathew et al., 2025), making cities less livable (Fung et al., 2024). Reported effects include increased water and energy consumption, decreased air quality, increased carbon emissions, and significant heat-related public health risks (Piracha and Chaudhary, 2022). However, the intensity of the effect can be influenced by environmental, climatic, and urban conditions (Liu et al., 2020), and follow patterns over long periods of time (Mohammad and Choi, 2023).

Among the most significant public health effects of SUHIs associated with high temperatures are alterations in the nervous system, cardiac or muscular problems, dehydration (Barrera et al., 2025), increased anxiety, exhaustion (Hossain et al., 2024), and death from heat waves related to SUHI (Heaviside et al., 2016), with the elderly and children, people with chronic diseases, and low-income households being the most vulnerable demographic groups (Ascencio et al., 2023; Ferguson and Anna, 2024), causing damage to metropolitan life in general (Gupta et al., 2020).

Thus, the effects may be related to the size of the metropolitan population (Cai et al., 2016), concentrated economic activities, industrial processes, and construction (Mathew et al., 2017). In addition, geographical factors can generate differences, with coastal cities generally suffering less from the consequences of SUHI than non-coastal cities (Smith et al., 2022), while the Global South suffers more in comparison than the Global North (Sadik and Gatto, 2022).

The effect of SUHI can be assessed and measured using various methods, but these can generally be divided into two main categories: (i) ground-based or field measurements, and (ii) satellite remote sensing, using specific thermal and shortwave bands (Mohamed et al., 2017). In the case of terrestrial measurement, the actual conditions of the terrain are defined using mobile devices or fixed stations (Hu et al., 2016). This procedure is specific and representative of small areas, and in most cases, it is difficult to integrate the spatial heterogeneity of the changes occurring in urban areas. It requires the use of numerous sensors within and around the city, skilled labor, and high implementation costs over long periods of time. (Patriota et al., 2024).

Therefore, satellite remote sensing can provide specialized information, such as land surface temperature (LST), which is more suitable for assessing SUHI events over long periods of time and large areas (Guo et al., 2024; Renc and Łupikasza, 2024; Yuan et al., 2023). In addition, when using LST data, two methods are generally chosen. The first consists of estimating the SUHI based on the division of urban and rural areas and the calculation of the difference in LST (Masoudi and Tan, 2019; Siddiqui et al., 2021). The second is based on using different statistical models to quantitatively calculate SUHI as Gaussian volume (Kumar et al., 2023). This study is of interest in order to explain the gradual increase in temperature in cities (Fan et al., 2017; Hathway and Sharples, 2012), and to better analyze the compression of its effects, allowing local authorities and cities to formulate plans and implement strategies to reduce damage and improve urban quality of life, especially in areas where the SUHI effect is expected to increase (Kundu et al., 2020).

The objective of this study is to analyze the temporal dynamics of SUHI at low resolution (0.05°) for the period 2001–2016 in the Metropolitan Region of Brasilia (MRG). The aim is to compare the Streutker (Streutker, 2002). and quantile (Flores et al., 2016) methods to detect patterns of diurnal and nocturnal variation and to determine the use of an

alternative statistical approach for polycentric cities that do not follow a Gaussian surface.

MATERIALS AND METHODS

Site and location

Located in southeastern South America, in Brazilian territory, is the Brasília Metropolitan Region (BMR), as shown in Figure 1A. The city has an average temperature of 21.6 °C and an annual rainfall of 1434.98 mm (Maciel, 2002).

During December 2001, the horizontal distribution of the monthly average surface temperature (MAST) across the entire BMR region is shown in Figures 1B and 1C, illustrating separately the diurnal and nocturnal patterns. The highest MAST recorded in the urban area of the BMR during that month was approximately 37 °C during the day, dropping to about 21 °C at night.

MODIS data

A monthly average was calculated with a resolution of up to 5 km, and a statistical analysis was performed of the effect of rescaling the LST statistical patterns and comparing them with the MOD11C3 Global CMG product (composite monthly average), based on the daily global MOD11C1 product, stored over a period of months at a resolution of 0.05° (5.6 km), using the MODIS sensor on the AQUA and TERRA satellites. A MODIS LST approach was implemented to eliminate the effects of non-vertical observation, urban geometry, subpixel variation in surface temperature, variable surface emissivity, and various atmospheric effects (Dousset and Gourmelon, 2003). This approach uses both daytime and nighttime measurements, taking advantage of the special features of the MODIS tool (Wan, 1999). Using seven-band thermal infrared (TIR) data (20, 22, 23, 29, and 31–33), the method recovers the average temperature and emissivity without the need for prior knowledge of the details of the temperature and water vapor profile (Wan and Li, 1997).

To differentiate between urban and rural landscapes, the MODIS land cover type (MCD12C1) product was used. This land cover classification tool (Figure 2) was created with a resolution of 0.05°. In this way, the landscape was categorized into the 17 land cover types of the International Geosphere-Biosphere Project (IGBP) (Schneider et al., 2003).

Relationship between LST and NDI and EVI

The normalized difference vegetation index (NDVI) stands out as the most widely used vegetation index. This metric emerged from observing
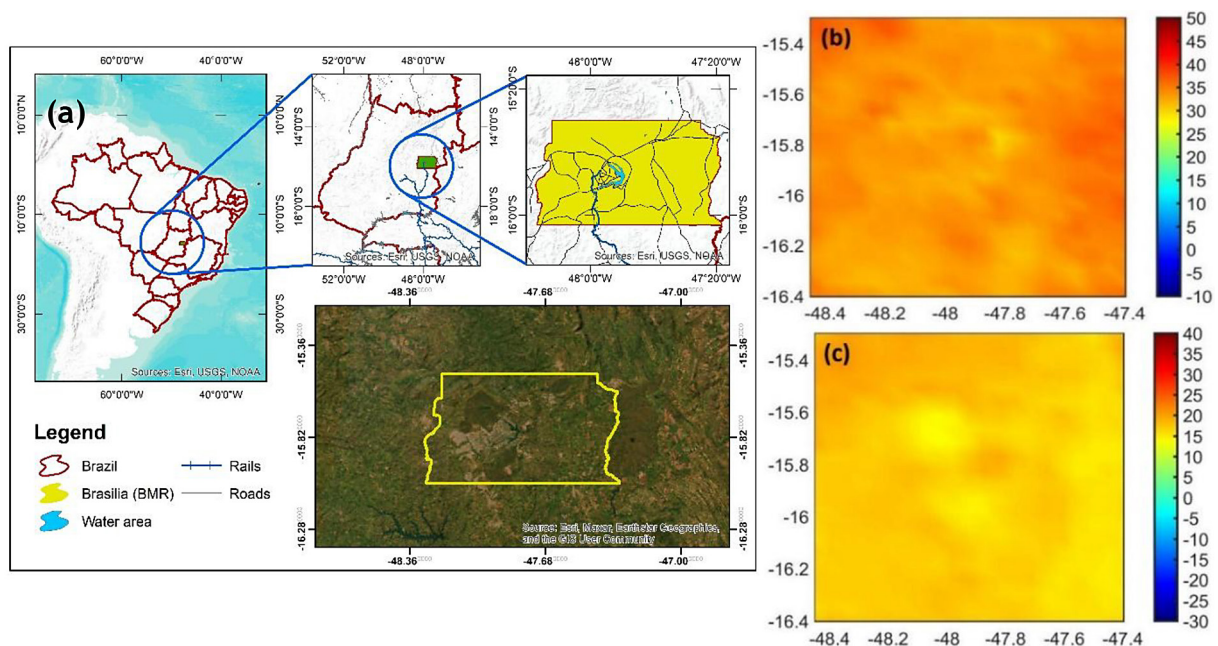

Figure 1. Distribution of horizontal surface temperature in the BMR. A) The BMR domain and B) the monthly average LST during the day and °C) nighttime periods in December 2001
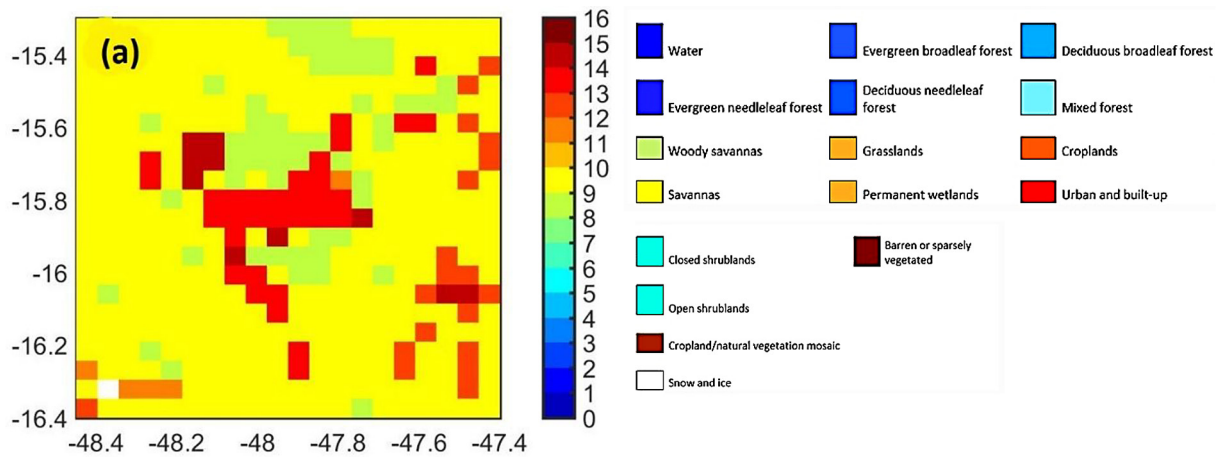
Figure 2. Type of ground cover in BMR

variations in the albedo of bare soil, with constant reflectance in red light (0.62–0.75 μm) and near-infrared (NIR, 0.75–1.4 μm), and areas covered by vegetation, which significantly increase NIR albedo compared to the visible part of the spectrum. In contrast, the enhanced vegetation index (EVI) refines the vegetation signal, increasing sensitivity where biomass is abundant and better monitoring vegetation by reducing atmospheric effects and separating the signal from the canopy background signal, as indicated in Equations 1 and 2 (Flores et al., 2016).

$$NDVI = \frac{NIR - red}{red + NIR} \tag{1}$$

$$EVI = G \times \\ \times \frac{NIR - red}{NIR + C_1 \times red - C_2 \times blue + L} \tag{2}$$

where: *red* (0.62–0.75 μm), *NIR* (0.75–1.4 μm), and *blue* (0.459–0.479 μm) are surface reflectance's that are corrected or partially corrected for atmospheric effects; *L* is the canopy background adjustment (nonlinear and differential transfer of red and *NIR* from the canopy); C_1 and C_2 are coefficients of the aerosol resistance term, which, adapted to MODIS-*EVI*, are: *G* (gain factor), $C_1 = 6$, $C_2 = 7.5$, and $L = 1$.

SUHI estimation

To determine the SUHI, the quantile method and the Streutker method proposed by Flores et al. (2016), and Streutker (2002), respectively, are used.

On the one hand, Streutke's approach, proposed in 2002, uses a Gaussian distribution to determine the intensity of the UHI effect in a spatial distribution. This pattern, based on a continuous change in LST, described in equations 3 and 4, calculates the intensity, centroid, shape, and spatial extent of SUHIs. All this is done to understand its magnitude and scope, without the need for local measurements. Since it analyzes the difference between city and countryside temperatures at the same time, it works well for studying many cities and also eliminates meteorological problems and other errors (Hung et al., 2006).

$$LST\,(x, y) = LST_0 + a_1 x + a_2 y + \\ + a_0\, exp\left(-\frac{(x - x_0)}{2\sigma_x^2} - \frac{(y - y_0)}{2\sigma_y^2}\right) \tag{3}$$

$$SUHI\,(x, y) = a_0\, exp \\ \left(-\frac{(x - x_0)}{2\sigma_x^2} - \frac{(y - y_0)}{2\sigma_y^2}\right) \tag{4}$$

where: the location of a pixel at (*x, y*) is indicated as *LST* (*x, y*). This value is divided into two parts: a constant value and a part that changes linearly with temperature. The background temperature is shown by $LST_0 + a_1 x + a_2 y$ (part of equation 2), and the SUHI pattern is represented by the remaining section (Equation 3). The combination of LST_0 is the average temperature in a rural area, and the coefficients (a_1 and a_2) describe the background temperature of a pixel (Streutker, 2003). To determine the longitudinal and latitudinal extensions of the SUHI, the parameters a_x and

a_y are used, respectively; for the centroid, they are x_0 and y_0; for the magnitude, it is a_0, which is the height of the Gaussian (Streutker, 2002). The area of each SUHI footprint with an adjusted Gaussian surface was approximated as the area of an ellipse as described below:

$$Footprint\ Area = \frac{\pi a'_x \times a'_y}{4} \quad (5)$$

where: based on the longitudinal (a_x) and latitudinal (a_y) extensions of the Gaussian model, the axes of the transformed ellipse are created, a'_x y a'_y.

In contrast, the quantile approach developed by Flores et al. (2016) uses a statistical quantile analysis of urban and rural land surface temperature. This is achieved by distinguishing urbanized areas using the MODIS MCD12C1 dataset, which has a resolution of 5 km. The monthly MODIS LST dataset, initially compiled every eight days (MOD11A2) with a resolution of 1 km, was rescaled to 5 km. This adjustment facilitates the separation of rural pixels from urban ones, allowing for a distinct statistical evaluation. In this way, unusual data are eliminated and the intensity of the lowest and highest LST readings is reduced. Based on this statistical work, the following formula was applied:

$$SUHI\ intensity = Q_5^{\text{urban}} - Q_3^{\text{rural}} \quad (6)$$

where: Q_3^{rural} is the median of the LST distribution over the rural area and Q_5^{urban} the 0.95 quartile of the urban area of the LST distribution, with a resolution of 5 km (Flores et al., 2016).

Thus, a statistical analysis of the LST was performed separately for urban and rural areas. As an example, Figure 3 shows the rural LST field for both daytime (Figure 3B) and nighttime (Figure 3C), and a box plot with quantiles (Figure 3A) for June 2015.

RESULTS AND DISCUSSION

Surface urban heat island (SUHI)

In the case of the centroid, $x_0 = -47.94$ and $y_0 = -15.76$ were used. Table 1 shows the daytime SUHI magnitudes, using the Streutker method,

compared to the surrounding areas of the BMR, and how far this heat extended in all months. The highest daytime temperature occurred in February (3.65 °C), while the lowest was observed in October (-1.53 °C). This result coincides with the study by Moreira et al. (2023), which indicates similar values during the local spring (41.9 °C and -3.2 °C in September and December, respectively), and an increase in LST over the years, indicating that vegetation cover was unable to reduce LST; However, for Campos et al. (2024), the highest peaks occur in the summer months on the coast of Brazil. In addition, Angeles et al. (2024) mention that negative values in the Streutker method are due to a contrary effect of the UHI, which is the result of cooling temperatures caused by sea breezes.

The maximum footprint area occurred in November (1.032 km^2) and the minimum in December (49 km^2). Table 1 also shows the correlation coefficient of the Gaussian fit (R^2) which was close to 0.10. Thus, increases in SUHI can occur homogeneously with respect to the growth of the spatial extent of urbanization (Kimothi et al., 2023). Although large areas are explained, it is necessary to take into account intra-urban variations, which, as indicated by Han et al. (2021), show notable variations in LST and intra-SUHI values when comparing parks and recreational areas with dense buildings.

To illustrate how the SUHI of the BMR changes throughout the year, Figure 4 shows the patterns of average annual surface temperature (both daytime and nighttime) in three different zones: urban, border, and rural. Graphs are shown describing the average temperatures recorded during 2001–2016, along with the standard deviation of the LST, for each of these three zones. In general, high temperature values in built-up areas are to be expected, due to the influence of concrete and asphalt (Portela et al., 2020), while solar radiation generates differences between daytime and nighttime SUHI (Athukorala and Murayama, 2020; Estoque et al., 2017).

The temporal evolution of the MAST for the daytime period (Figure 4A), where the maximum MAST for this period is observed in September for the urban (35 °C), border (35 °C), and rural areas (34 °C), while the minimum average values are observed in April for the urban (27 °C), border (28 °C), and rural areas (26 °C). These can mostly occur early in the morning and at midday or in the afternoon, related to urban geometry, and
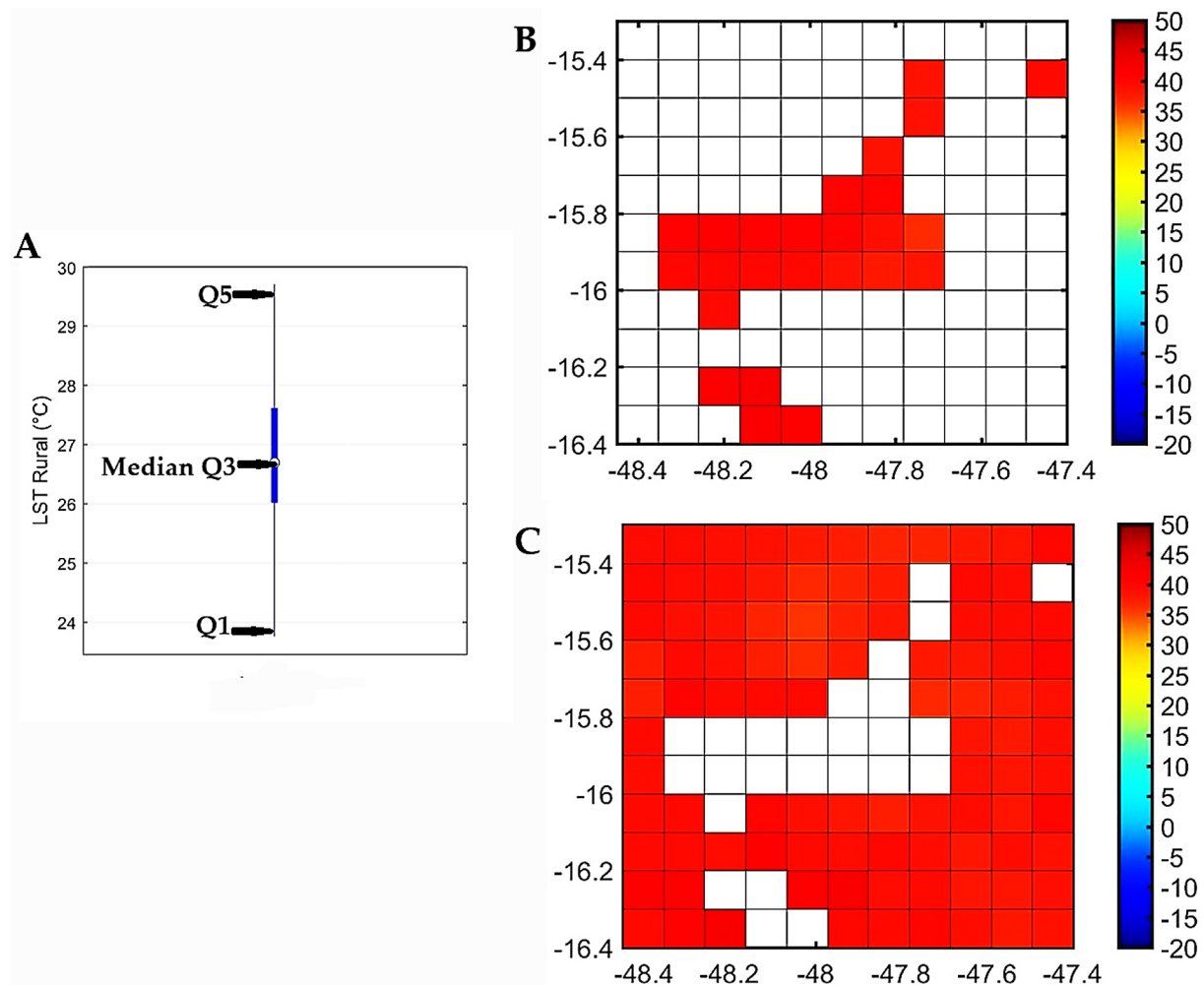
Figure 3. Boxplot diagram for values of LST showed in A), indicating quantile 0.05 (Q1), median (Q3), quantile 0.95 (Q5), B) Mean monthly diurnal LST (5 km resolution) over the urban area of the BMR for June 2015. (Q4) and quantile 0.95 (Q5) y C) Mean monthly diurnal LST over the rural area of the BMR for June 2015.

these results are in line with those mentioned by Lai et al. (2018). Diurnal variations in LST are mainly driven by shortwave radiation, but vegetation types also generate notable differences: cropland has a high LST value, followed by scrubland and grassland, with forests having the lowest value (making them a candidate for mitigating SUHI) (Wang et al., 2025).

At night, the temporal evolution of the MAST (Figure 4B), with maximum values in October for the urban (20 °C), border (19 °C) and rural areas (18 °C), unlike the minimum average values observed in July for the urban (17 °C), border (16 °C) and rural areas (16 °C). In the case of large cities, such as Brasilia, the absorption of electromagnetic energy by buildings and the proportion of vegetation can enhance the nighttime effect (Almeida and Teodoro, 2020); it can also

affect medium-sized cities with different climatic conditions and urban expansion factors than those in this study, such as Akure and Osogbo, located in Nigeria (Oyeniyi et al., 2025). However, as indicated by Li et al. (2025), as the urban area expands, the nighttime SUHI tends to decrease. This may be due to the thermal inertia of urban materials that influence the nighttime SUHI, where smaller cities have a higher ISR, which potentially amplifies it (Li et al., 2020).

SUHI during the day and night

In Figure 5A, a scatter plot compares the two methods across all months. A linear regression analysis reveals a slope of 0.98 and an intersection of -0.48, with a correlation coefficient of 0.12. Furthermore, in the nighttime period (Figure 5B),

Table 1. Mean SUHI intensity and spatial coverage, including standard deviation, for the BMR estimated using the Streutker (2002) approach during the period 2001–2016

Month	LST$_0$ (°C)	a$_0$ (°C)	a'$_x$ (km)	a'$_y$(km)	Footprint area (km^2)	R^2
January	27.23 ± 1.96	2.81 ± 1.17	3.16 ± 32.15	8.73 ± 6.11	74.5 ± 127.4	0.08
February	27.51 ± 1.73	3.65 ± 2.38	12.23 ± 6.76	8.68 ± 5.39	119.7 ± 143.9	0.12
March	26.51 ± 1.63	2.96 ± 0.95	10.82 ± 3.92	5.44 ± 1.30	58.9 ± 25.9	0.06
April	26.93 ± 1.68	2.37 ± 0.83	11.29 ± 4.32	4.48 ± 2.33	54.9 ± 37.9	0.05
May	26.98 ± 1.23	1.90 ± 0.92	6.47 ± 10.54	1.67 ± 5.55	64.1 ± 72.9	0.04
June	26.76 ± 1.04	1.74 ± 1.13	7.31 ± 10.24	4.28 ± 4.16	70.4 ± 54.2	0.03
July	28.31 ± 1.03	1.72 ± 2.12	-0.29 ± 13.56	1.23 ± 6.50	80.2 ± 72.3	0.02
August	31.59 ± 1.03	1.69 ± 1.51	-3.71 ± 15.34	-8.93 ± 33.46	332.2 ± 812	0.03
September	34.98 ± 1.78	0.93 ± 1.92	-4.55 ± 37.79	2.75 ± 15.47	247 ± 524.7	0.06
October	34.88 ± 3.30	-1.53 ± 2.78	7.49 ± 13.08	76.06 ± 184.36	848.1 ± 2,433.8	0.13
November	30.28 ± 2.08	-0.01 ± 1.86	12.43 ± 10.47	60.66 ± 191.88	1,032.5 ± 3,084.1	0.07
December	28.91 ± 2.18	1.57 ± 2.90	20.89 ± 30.05	2.46 ± 41.32	49.2 ± 1,161.2	0.06

Note: The table shows the verage temperature for rural area LST$_0$ (°C), SUHI magnitude: α_0 (°C), longitudinal extent: a'$_x$ (km), latitudinal extent: a'$_y$ (km), footprint area (km^2), and R-squared fit.
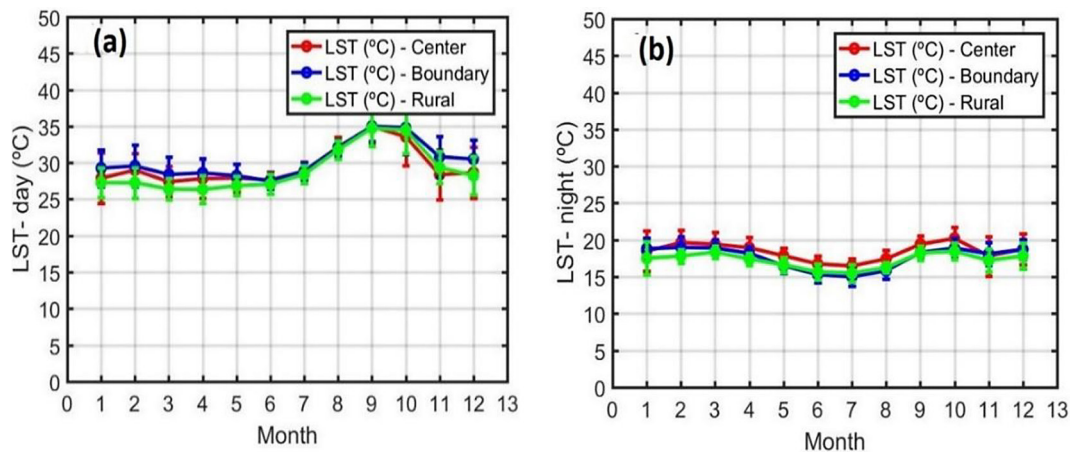
Figure 4. Temporal evolution of MAST of the BMR in urban areas (red lines), border areas (blue line), and rural areas (green line). A) Daytime period and B) nighttime period

the linear fit gives a slope of 1.12 and an intersection of 0.95, along with a correlation index of 0.14. The temporal variation of NDVI and EVI is the cause of this relationship (Angeles et al., 2019). Applying other methods also confirms a positive trend of gradual increase in SUHIs in Brazil, where latitude, population, and biome type are factors that explain diurnal and nocturnal variations (Patriota et al., 2024).

Table 2 presents the results of the BMR, based on the quantile method focused on daytime quantiles. The upper quantile (Q5) of the urban MAST reached its maximum in September, with 36.72 °C, while the minimum was recorded in June, with 28.28 °C. The highest average rural LST (Q3) occurred in September,

reaching 34.89 °C, while the lowest was recorded in March, at 26.51 °C. The daytime SUHI reached its highest point in January (3.08 °C) and its lowest in July (1.51 °C). These values may be susceptible to impervious surfaces, bare earth, and green spaces (Athukorala and Murayama, 2021), which can affect daytime and nighttime values on a monthly and regional basis (Lai et al., 2018).

During the nighttime period, as shown in Table 3 and Figure 5A, the highest quantile value (Q5) for urban MAST was observed in October (20.45 °C) and the lowest in July (16.49 °C). The highest mean value for rural MAST (Q3) was observed in October (18.43 °C) and the lowest in July (14.13 °C). The nighttime SUHI shows maximum values in July (2.36 °C) and
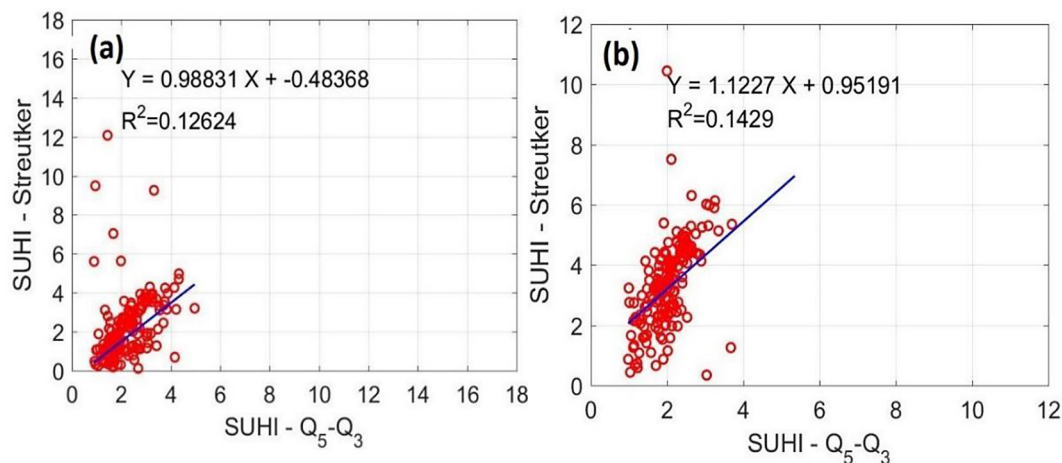
Figure 5. Scatter plot of SUHI, obtained by the Streutker method versus SUHI with the difference in quantiles ($Q_5^{urban} - Q_3^{rural}$): a) daytime period, b) nighttime period

Table 2. Monthly average daytime LST (°C) for rural and urban areas and SUHI intensity (°C) at 5 km resolution for BMR during the period 2001–2016

Month	Q_3 (Urban LST)	Q_5 (Urban LST)	Q_3 (Rural LST)	Q_5 (Rural LST)	SUHI Diurnal (°C)
January	28.42 ± 2.31	30.37 ± 2.13	27.29 ± 2.05	29.31 ± 2.07	3.08 ± 0.81
February	28.74 ± 2.05	30.55 ± 2.35	27.54 ± 1.77	29.25 ± 1.79	3.01 ± 0.83
March	27.39 ± 1.81	29.06 ± 1.93	26.51 ± 1.62	28.46 ± 1.80	2.55 ± 0.53
April	27.63 ± 1.93	29.03 ± 2.03	26.88 ± 1.67	28.97 ± 1.81	2.15 ± 0.48
May	27.41 ± 1.44	28.81 ± 1.53	26.85 ± 1.26	28.99 ± 1.29	1.96 ± 0.59
June	27.20 ± 1.11	28.28 ± 1.17	26.67 ± 1.06	28.45 ± 1.14	1.61 ± 0.45
July	28.72 ± 1.17	29.76 ± 1.34	28.25 ± 1.08	30.10 ± 1.08	1.51 ± 0.47
August	32.16 ± 1.14	33.25 ± 1.28	31.55 ± 1.06	33.54 ± 1.06	1.70 ± 0.34
September	35.29 ± 2.08	36.72 ± 2.13	34.89 ± 1.89	37.38 ± 1.81	1.83 ± 0.54
October	34.72 ± 3.64	36.61 ± 3.55	34.71 ± 3.33	37.76 ± 3.67	1.90 ± 0.48
November	30.38 ± 2.29	32.45 ± 2.21	30.19 ± 2.07	33.46 ± 2.43	2.26 ± 0.71
December	29.41 ± 2.33	31.65 ± 2.42	28.82 ± 2.19	31.48 ± 2.44	2.84 ± 0.95

Note: The table shows values for the median Q_3 and the 0.95 quantile Q_5.

minimum values in April (1.72 °C). Compared to other cities that are not part of the urban center, such as São João de Pirabas in Brazil, the SUHI intensifies more at night than during the day due to the air temperature and relative humidity in the early hours of the day (Do Vale et al., 2025), as is the case in small cities, mentioned by Li et al. (2025). However, Monteiro et al. (2021), found that the Metropolitan Region of Brasília has more intense nighttime SUHI than daytime SUHI, compared to other cities in the same country, mainly in the dry season, due to intense verticalization, urban density, and the thermal properties of building materials.

These values are shown in Figure 6B in contrast to the daytime case, where it can be seen

that the intensity of the nighttime SUHI is lower. These characteristics may be due to the fact that as the urban area increases, the SUHI increases steadily over evaluation periods similar to those in this study (Chen et al., 2020). In the case of Li et al. (2025), in warmer climatic zones, the daytime SUHI is more intense, while the nighttime SUHI values are high in arid regions.

According to Figure 6C, variations can be identified in the period studied, which means changes in the horizontal and vertical structure of the city of Brasilia, influencing SUHI values in both methods. This information is related to Nova et al. (2021), since urbanization can vary over long periods of time and ultimately the effects of SUHI. These effects can be related to

Table 3. Monthly average nighttime LST (°C) for rural and urban areas and SUHI intensity (°C) at 5 km resolution for the BMR during 2001–2016

Month	Q_3 (Urban LST)	Q_5 (Urban LST)	Q_3 (Rural LST)	Q_5 (Rural LST)	SUHI Nocturnal (°C)
January	18.47 ± 1.44	20.14 ± 0.99	18.01 ± 1.34	20.12 ± 0.94	2.13 ± 0.96
February	18.64 ± 1.08	20.17 ± 1.17	18.10 ± 0.83	19.84 ± 0.96	2.07 ± 0.45
March	18.70 ± 1.01	20.09 ± 1.21	18.28 ± 0.80	19.92 ± 0.99	1.81 ± 0.65
April	18.02 ± 0.99	19.32 ± 1.00	17.60 ± 0.75	19.39 ± 0.86	1.72 ± 0.59
May	16.41 ± 0.93	17.85 ± 1.03	15.81 ± 0.78	18.08 ± 0.87	2.04 ± 0.45
June	15.29 ± 0.88	16.88 ± 1.00	14.59 ± 0.81	17.10 ± 0.86	2.29 ± 0.41
July	14.95 ± 1.02	16.49 ± 0.95	14.13 ± 0.82	16.83 ± 0.76	2.36 ± 0.31
August	15.95 ± 1.00	17.46 ± 1.03	15.17 ± 0.91	17.92 ± 0.76	2.29 ± 0.39
September	18.17 ± 0.83	19.42 ± 0.93	17.44 ± 0.72	19.91 ± 0.71	1.98 ± 0.46
October	18.93 ± 1.20	20.45 ± 1.18	18.43 ± 0.81	20.52 ± 0.94	2.02 ± 0.46
November	18.03 ± 1.23	19.65 ± 1.15	17.85 ± 1.02	20.03 ± 1.13	1.80 ± 0.46
December	18.68 ± 1.17	20.22 ± 1.12	18.22 ± 1.17	20.37 ± 1.16	2.00 ± 0.76

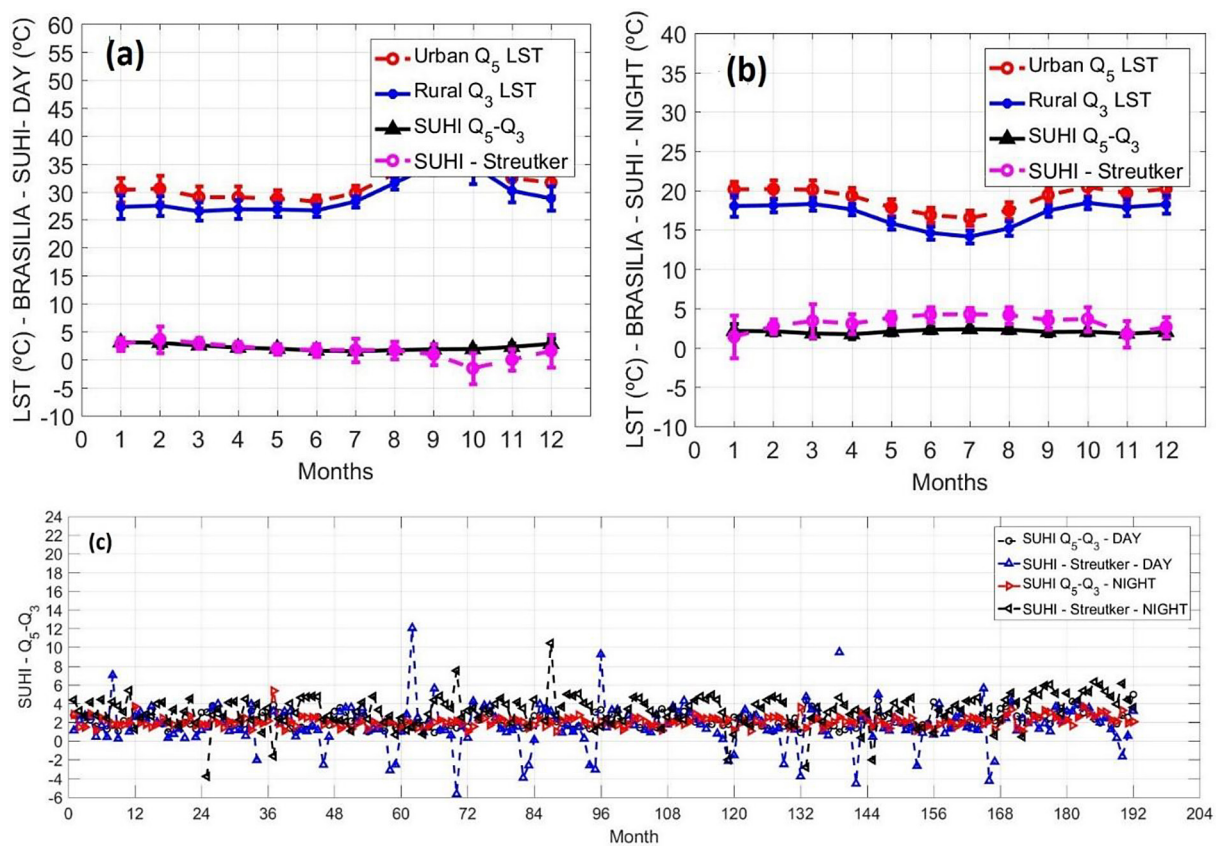**Note**: The table shows values for the median Q_3 and the 0.95 quantile Q_5.

Figure 6. Temporal evolution from 2001 to 2016, monthly average LST (°C) with standard deviation for the LST period for BMR: a) daytime period, b) nighttime period, c) SUHI intensity (°C)

patterns of land use change, such as commercial and residential areas and lack of green spaces (Barbosa and Dutra, 2024). Therefore, vegetated land can help mitigate the effects, serving as an alternative for sustainable urban growth (Kimothi et al., 2023).

CONCLUSIONS

The analysis revealed that the Brasília Metropolitan Region exhibits diurnal and nocturnal variability in the SUHI, reaching its maximum during the day in January, with 3.08 °C, and

falling to its minimum in July, with 1.51 °C. In contrast, during the night, the highest SUHI values are recorded in July, at 2.36 °C, while the lowest are observed in April, at 1.72 °C.

In contrast, the comparison of SUHI between the quantile and Streutker methods yielded a low correlation close to 0.10, as the BMR does not fit a Gaussian surface, making the quantile method essential. Therefore, the traditional Gaussian approximation is not suitable for cities with multiple thermal hotspots, while the quantile method proved to be more robust in capturing the spatial heterogeneity of surface temperature, complementing the Streutker method for cities with more than one maximum surface temperature center.

It is important to mention that the heterogeneity of urban areas, due to variations in topography and altitude, can influence verticalization, generating uncertainties in the estimation of LST and therefore SUHI. In addition, the azimuth and zenith angles of each pixel are unique, which causes the geometric view of a city's thermal image to be diverse. Therefore, to address this problem, it is recommended that future studies include LST data with better resolutions (less than 1 km), provided that they comply with the corresponding time series (annual and monthly).

REFERENCES

1. Abdullah, S., Al-Alwan, H. (2019). Urban resilience in the sustainable urban regeneration of historic city centers. *Association of Arab Universities Journal of Engineering Sciences*, *26*(4), 130–143. https://doi.org/10.33261/JAARU.2019.26.4.015

2. Almeida, C., Teodoro, A. (2020). Relationship between the land surface temperature and the vegetation proportion to identify heat islands: case study of Brasília (Brazil). *11534*, 230–241. https://doi.org/10.1117/12.2572802

3. Angeles, J., Angeles, R., Lavado, C., de la Cruz, L., Angeles, N., Flores, J., Abi, H. (2024). Superficial urban heat island in the metropolitan area of Grande Vitoria/Brazil. *Proceedings of the LACCEI International Multi-Conference for Engineering, Education and Technology*. https://doi.org/10.18687/LACCEI2024.1.1.298

4. Angeles, J., Vasques, R., Rojas, J. L., Karam, H. (2019). Estimación de Isla de Calor Urbana Superficial en el Area Metropolitana de Iquitos/Peru. *Anuário Do Instituto de Geociências*, *42*(1), 135–145. https://doi.org/10.11137/2019_1_135_145

5. Ascencio, E. J., Barja, A., Benmarhnia, T., Carrasco-Escobar, G. (2023). Disproportionate exposure to surface-urban heat islands across vulnerable populations in Lima city, Peru. *Environmental Research Letters*, *18*(7). https://doi.org/10.1088/1748-9326/ACDCA9

6. Athukorala, D., Murayama, Y. (2020). Spatial variation of land use/cover composition and impact on surface urban heat island in a tropical Sub-Saharan City of Accra, Ghana. *Sustainability 12*(19), 7953. https://doi.org/10.3390/SU12197953

7. Athukorala, D., Murayama, Y. (2021). Urban heat island formation in greater Cairo: Spatio-Temporal analysis of daytime and nighttime land surface temperatures along the urban–rural gradient. *Remote Sensing 13*(7), 1396. https://doi.org/10.3390/RS13071396

8. Banzhaf, E., Roig, H. L., Bakker, F. (2009). Characterising the phenomenon of water scarcity in the fast growing federal district of Brasilia. *2009 Joint Urban Remote Sensing Event*. https://doi.org/10.1109/URS.2009.5137477

9. Barbosa, P. L., Dutra, F. N. (2024). Multivariate Analysis of the Urban Heat Island of the Metropolitan Area of São Paulo, Brazil. *Revista Brasileira de Meteorologia*, *39*. https://doi.org/10.1590/0102-77863910045

10. Barrera, I., Tapia-McClung, R., Caudillo Cos, C., Arvizu Piña, V., Montejano-Escamilla, J. A. (2025). Vulnerable population and risk areas to the surface urban heat island phenomenon and their accessibility to healthcare. The 15 warmest Mexican cities. *International Journal of Cartography*. https://doi.org/10.1080/23729333.2025.2521567;CSUBTYPE:STRING:AHEAD

11. Brazilian Institute of Geography and Statistics [IGBE]. (2025). *IBGE | Ciudades | Distrito Federal | Brasilia | Panorama*. https://cidades.ibge.gov.br/brasil/df/brasilia/panorama

12. Cai, Y., Zhang, H., Zheng, P., Pan, W. (2016). Quantifying the impact of land use/land cover changes on the urban heat island: A case study of the natural wetlands distribution area of Fuzhou City, China. *Wetlands*, *36*(2), 285–298. https://doi.org/10.1007/S13157-016-0738-7/METRICS

13. Campos, C. W., Rosales Aylas, G. Y., Magalhães Santiago, A., do Vale, C. C., Silva, M. E. S., da Silva, C. B., Nascentes Coelho, A., Lima Freire, A. H., Mataveli, G., Martins Moreira, D. (2024). Temporal and spatial urban heat islands in a Coastal Brazilian Area of Tropical Climate. *Papers in Applied Geography*, *10*(2), 114–137. https://doi.org/10.1080/23754931.2024.2321561;REQUESTEDJOURNAL:JOURNAL:RPAG20;SUBPAGE:STRING:ACCESS

14. Chen, M., Zhou, Y., Hu, M., Zhou, Y. (2020). Influence of urban scale and urban expansion on the urban heat island effect in metropolitan areas: Case study of Beijing–Tianjin–Hebei urban agglomeration. *Remote Sensing 12*(21), 3491. https://doi.org/10.3390/RS12213491

15. Costa, C., Lee, S. (2019). The evolution of urban spatial structure in Brasília: Focusing on the role of urban development policies. *Sustainability 11*(2), 553. https://doi.org/10.3390/SU11020553

16. Do Vale, E. M. V., Barros, L. R. C., Barral, E. C. V., Soeiro, J. C., Brandão, J. M. A., Xavier, L. O., da Silva, A. L. O., Oliveira, L. C. G., Rodrigues, H. J. B., Filho, J. D. da C. S., Ribeiro, J. B. M., Gomes, D. J. C., de Lima, A. M. M., de Moraes, B. C., Junior, J. de A. S. (2025). Urban heat island in São João de Pirabas - PA. *Revista Brasileira de Geografia Fisica*, *18*(1), 95–108. https://doi.org/10.26848/RBGF.V18.1.P095-108

17. Dousset, B., Gourmelon, F. (2003). Satellite multisensor data analysis of urban surface temperatures and landcover. *ISPRS Journal of Photogrammetry and Remote Sensing*, *58*(1–2), 43–54. https://doi.org/10.1016/S0924-2716(03)00016-9

18. Estoque, R. C., Murayama, Y., Myint, S. W. (2017). Effects of landscape composition and pattern on land surface temperature: An urban heat island study in the megacities of Southeast Asia. *Science of The Total Environment*, *577*, 349–359. https://doi.org/10.1016/J.SCITOTENV.2016.10.195

19. Fan, C., Myint, S. W., Kaplan, S., Middel, A., Zheng, B., Rahman, A., Huang, H. P., Brazel, A., Blumberg, D. G. (2017). Understanding the impact of urbanization on surface urban heat islands—A longitudinal analysis of the oasis effect in subtropical desert cities. *Remote Sensing*, *9*(7), 672. https://doi.org/10.3390/RS9070672

20. Ferguson, L., Anna, M. (2024). The impact of heat adaptation on socioeconomically vulnerable populations. *Mitigation and Adaptation of Urban Overheating: The Impact of Warmer Cities on Climate, Energy, Health, Environmental Quality, Economy, and Quality of Life*, 277–293. https://doi.org/10.1016/B978-0-443-13502-6.00010-5

21. Flores, J. L., Pereira Filho, A. J., Karam, H. A. (2016). Estimation of long term low resolution surface urban heat island intensities for tropical cities using MODIS remote sensing data. *Urban Climate*, *17*, 32–66. https://doi.org/10.1016/J.UCLIM.2016.04.002

22. Fraser, V. (2004). Brasília. *Readings in Latin American Modern Art*, 117–131. https://doi.org/10.3917/VING.081.0093

23. Fung, K. Y., Yang, Z. L., Martilli, A., Krayenhoff, E. S., Niyogi, D. (2024). Prioritizing social vulnerability in urban heat mitigation. *PNAS Nexus*, *3*(9). https://doi.org/10.1093/PNASNEXUS/PGAE360

24. Guo, F., Sun, J., Hu, D. (2024). Surface energy balance-based surface urban heat island decomposition at high resolution. *Remote Sensing of Environment*, *315*. https://doi.org/10.1016/J.RSE.2024.114447

25. Gupta, N., Mathew, A., Khandelwal, S. (2020). Spatio-temporal impact assessment of land use / land cover (LU-LC) change on land surface temperatures over Jaipur city in India. *International Journal of Urban Sustainable Development*, *12*(3), 283–299. https://doi.org/10.1080/19463138.2020.1727908

26. Han, J., Zhao, X., Zhang, H., Liu, Y. (2021). Analyzing the Spatial Heterogeneity of the Built Environment and Its Impact on the Urban Thermal Environment—Case Study of Downtown Shanghai. *Sustainability 2021, Vol. 13, Page 11302*, *13*(20), 11302. https://doi.org/10.3390/SU132011302

27. Hathway, E. A., Sharples, S. (2012). The interaction of rivers and urban form in mitigating the Urban Heat Island effect: A UK case study. *Building and Environment*, *58*, 14–22. https://doi.org/10.1016/J.BUILDENV.2012.06.013

28. Heaviside, C., Vardoulakis, S., Cai, X. M. (2016). Attribution of mortality to the urban heat island during heatwaves in the West Midlands, UK. *Environmental Health: A Global Access Science Source*, *15*. https://doi.org/10.1186/S12940-016-0100-9

29. Hossain, I., Rana, M. S., Haque, A. K. M. M., Al Masud, A. (2024). Urban household adaptation to extreme heatwaves: health impacts, socio-economic disparities and sustainable strategies in Rajshahi. *Discover Sustainability*, *5*(1), 1–18. https://doi.org/10.1007/S43621-024-00697-2/TABLES/4

30. Hu, X. M., Xue, M., Klein, P. M., Illston, B. G., Chen, S. (2016). Full access analysis of urban effects in Oklahoma city using a dense surface observing network. *Journal of Applied Meteorology and Climatology*, *55*(3), 723–741. https://doi.org/10.1175/JAMC-D-15-0206.1

31. Hung, T., Daisuke, U., Shiro, O., Yoshifumi, Y. (2006). Assessment with satellite data of the urban heat island effects in Asian mega cities. *International Journal of Applied Earth Observation and Geoinformation*, *8*(1), 34–48. https://doi.org/10.1016/J.JAG.2005.05.003

32. Kimothi, S., Thapliyal, A., Gehlot, A., Aledaily, A. N., gupta, A., Bilandi, N., Singh, R., Kumar Malik, P., Vaseem Akram, S. (2023). Spatio-temporal fluctuations analysis of land surface temperature (LST) using Remote Sensing data (LANDSAT TM5/8) and multifractal technique to characterize the urban heat Islands (UHIs). *Sustainable Energy Technologies and Assessments*, *55*, 102956. https://doi.org/10.1016/J.SETA.2022.102956

33. Kumar, A., Mukherjee, M., Goswami, A. (2023). Inter-seasonal characterization and correlation of Surface Urban Heat Island (SUHI) and Canopy Urban Heat Island (CUHI) in the urbanized environment of Delhi. *Remote Sensing Applications: Society and Environment*, *30*, 100970. https://doi.org/10.1016/J.RSASE.2023.100970

34. Kundu, D., Sietchiping, R., Kinyanjui, M. (2020). Developing National Urban Policies: Ways Forward to

Green and Smart Cities. *Developing National Urban Policies: Ways Forward to Green and Smart Cities*, 1–450. https://doi.org/10.1007/978-981-15-3738-7/COVER

35. Lai, J., Zhan, W., Huang, F., Voogt, J., Bechtel, B., Allen, M., Peng, S., Hong, F., Liu, Y., Du, P. (2018). Identification of typical diurnal patterns for clear-sky climatology of surface urban heat islands. *Remote Sensing of Environment*, *217*, 203–220. https://doi.org/10.1016/J.RSE.2018.08.021

36. Leonardo, H. R. de A. L., Almeida, D. N. O. de, Amorim, A. R. de, Paiva, A. L. R. de, Oliveira, L. M. M. de, Santos, S. M. Dos. (2025). Remote sensing applied to biophysical parameters and land cover to identify urban heat islands in Recife (PE), Brazil. *Revista Brasileira de Ciencias Ambientais*, *60*. https://doi.org/10.5327/Z2176-94782107

37. Li, S., Liang, Y., Yang, D., Shen, J. (2025). Effect of blue-green landscape pattern and urban forms on surface urban heat island intensity: Evidence from 816 Chinese urban clusters. *Ecological Indicators*, *178*, 113949. https://doi.org/10.1016/J.ECOLIND.2025.113949

38. Li, Y., Schubert, S., Kropp, J. P., Rybski, D. (2020). On the influence of density and morphology on the Urban Heat Island intensity. *Nature Communications*, *11*(1). https://doi.org/10.1038/S41467-020-16461-9

39. Liu, Y., Li, Q., Yang, L., Mu, K., Zhang, M., Liu, J. (2020). Urban heat island effects of various urban morphologies under regional climate conditions. *Science of The Total Environment*, *743*, 140589. https://doi.org/10.1016/J.SCITOTENV.2020.140589

40. Maciel, A. (2002). *Projeto Bioclimático em Brasília: Estudo de Caso em Edifício de Escritórios* [Dissertação apresentada ao curso de Pós Graduação em Engenharia Civil para a obtenção do Título de Mestre em Engenharia Civil [Mestre, Universidad Federal de Santa Catarina], Universidad Federal de Santa Catarina]. https://repositorio.ufsc.br/handle/123456789/82350

41. Masoudi, M., Tan, P. Y. (2019). Multi-year comparison of the effects of spatial pattern of urban green spaces on urban land surface temperature. *Landscape and Urban Planning*, *184*, 44–58. https://doi.org/10.1016/J.LANDURBPLAN.2018.10.023

42. Mathew, A., Aljohani, T. H., Shekar, P. R., Arunab, K. S., Sharma, A. K., Ahmed, M. F. M., Idris, U. I. A., Almohamad, H., Abdo, H. G. (2025). Spatiotemporal dynamics of urban heat island effect and air pollution in Bengaluru and Hyderabad: implications for sustainable urban development. *Discover Sustainability*, *6*(1), 1–26. https://doi.org/10.1007/S43621-025-00860-3/TABLES/7

43. Mathew, A., Khandelwal, S., Kaul, N. (2017). Investigating spatial and seasonal variations of urban heat island effect over Jaipur city and its relationship with vegetation, urbanization and elevation parameters. *Sustainable Cities and Society*, *35*, 157–177. https://doi.org/10.1016/J.SCS.2017.07.013

44. Mirabi, E., Davies, P. J. (2022). A systematic review investigating linear infrastructure effects on Urban Heat Island (UHIULI) and its interaction with UHI typologies. *Urban Climate*, *45*, 101261. https://doi.org/10.1016/J.UCLIM.2022.101261

45. Mohamed, A. A., Odindi, J., Mutanga, O. (2017). Land surface temperature and emissivity estimation for Urban Heat Island assessment using medium- and low-resolution space-borne sensors: A review. *Geocarto International*, *32*(4), 455–470. https://doi.org/10.1080/10106049.2016.1155657

46. Mohammad Harmay, N. S., Choi, M. (2023). The urban heat island and thermal heat stress correlate with climate dynamics and energy budget variations in multiple urban environments. *Sustainable Cities and Society*, *91*, 104422. https://doi.org/10.1016/J.SCS.2023.104422

47. Monteiro, F. F., Gonçalves, W. A., Andrade, L. de M. B., Villavicencio, L. M. M., dos Santos Silva, C. M. (2021). Assessment of urban heat islands in Brazil based on MODIS remote sensing data. *Urban Climate*, *35*, 100726. https://doi.org/10.1016/J.UCLIM.2020.100726

48. Moreira, C. M., Rezende, A. V., Sano, E. E., Trondoli, E. A., Delgado, R. C. (2023). Spatiotemporal assessment of land surface temperature and vegetation in tropical urban areas. *Urban Ecosystems*, *26*(1), 45–65. https://doi.org/10.1007/S11252-022-01276-X/METRICS

49. Nova, R. A. V., Goncalves, R. M., Lima, F. V. M. S. (2021). Temporal analysis of heat islands through surface temperature and vegetation index in Recife-PE, Brazil. *Revista Brasileira de Cartografia*, *73*(2), 598–614. https://doi.org/10.14393/RBCV73N2-54522

50. Oyeniyi, M. A., Odunsi, O. M., Rienow, A., Edler, D. (2025). Spatiotemporal analysis of land use change and urban heat island effects in Akure and Osogbo, Nigeria Between 2014 and 2023. *Climate 13*(4), 68. https://doi.org/10.3390/CLI13040068

51. Parece, T. E., Li, J., Campbell, J. B., Carroll, D. (2016). Assessing Urban Landscape Variables' Contributions to Microclimates. *Advances in Meteorology*, *2016*(1), 8736263. https://doi.org/10.1155/2016/8736263

52. Patriota, E. G., Bertrand, G. F., Almeida, C. das N., Claudino, C. M. de A., Coelho, V. H. R. (2024). Heat the road again! Twenty years of surface urban heat island intensity (SUHII) evolution and forcings in 21 tropical metropolitan regions in Brazil from remote sensing analyses. *Sustainable Cities and Society*, *113*, 105629. https://doi.org/10.1016/J.SCS.2024.105629

53. Piracha, A., Chaudhary, M. T. (2022). Urban air pollution, urban heat island and human health: a review of the literature. *Sustainability 14*(15), 9234. https://doi.org/10.3390/SU14159234

54. Portela, C. I., Massi, K. G., Rodrigues, T., Alcântara, E. (2020). Impact of urban and industrial features on land surface temperature: Evidences from satellite thermal indices. *Sustainable Cities and Society*, *56*, 102100. https://doi.org/10.1016/J.SCS.2020.102100

55. Renc, A., Łupikasza, E. (2024). Permanent and seasonally specific surface heat island structure in urban and non-urban areas in mid-latitude polycentric agglomeration based on Landsat images. *Ecological Indicators*, *169*. https://doi.org/10.1016/J.ECOLIND.2024.112871

56. Reyes, M., Aguiluz, J. (2023). Relevant factors on the formation of heat islands in the Metropolitan Zone of Querétaro. *Legado de Arquitectura y Diseno*, *18*(33), 7–16. https://doi.org/10.36677/LEGADO.V18I33.17416

57. Sadik, E. R., Gatto, A. (2022). Vulnerability to the urban heat islands effect in the Global North and the Global South: assessment of the drivers and mitigation strategies. *Global Urban Heat Island Mitigation*, 29–45. https://doi.org/10.1016/B978-0-323-85539-6.00012-3

58. Schneider, A., Friedl, M. A., Woodcock, C. E. (2003). Mapping urban areas by fusing multiple sources of coarse resolution remotely sensed data. *International Geoscience and Remote Sensing Symposium (IGARSS)*, *4*, 2623–2625. https://doi.org/10.1109/IGARSS.2003.1294530

59. Siddiqui, A., Kushwaha, G., Nikam, B., Srivastav, S. K., Shelar, A., Kumar, P. (2021). Analysing the day/night seasonal and annual changes and trends in land surface temperature and surface urban heat island intensity (SUHII) for Indian cities. *Sustainable Cities and Society*, *75*. https://doi.org/10.1016/J.SCS.2021.103374

60. Smith, P., Sarricolea, P., Peralta, O., Toro, C. (2022). Surface urban heat islands in 33 medium-sized cities across different climates in Chile. *Global Urban Heat Island Mitigation*, 323–334. https://doi.org/10.1016/B978-0-323-85539-6.00004-4

61. Streutker, D. R. (2002). A remote sensing study of the urban heat island of Houston, Texas. *International Journal of Remote Sensing*, *23*(13), 2595–2608. https://doi.org/10.1080/01431160110115023

62. Streutker, D. R. (2003). Satellite-measured growth of the urban heat island of Houston, Texas. *Remote Sensing of Environment*, *85*(3), 282–289. https://doi.org/10.1016/S0034-4257(03)00007-5

63. Tawfeeq Najah, F., Fakhri Khalaf Abdullah, S., Ameen Abdulkareem, T. (2023). Urban land use changes: effect of green urban spaces transformation on urban heat islands in Baghdad. *Alexandria Engineering Journal*, *66*, 555–571. https://doi.org/10.1016/J.AEJ.2022.11.005

64. Wan, Z. (1999). MODIS Land-Surface Temperature Algorithm Theoretical Basis Document (LST ATBD). In *Institute for Computational Earth System Science, Santa Barbara*.

65. Wan, Z., Li, Z. L. (1997). A physics-based algorithm for retrieving land-surface emissivity and temperature from eos/modis data. *IEEE Transactions on Geoscience and Remote Sensing*, *35*(4), 980–996. https://doi.org/10.1109/36.602541

66. Wang, W., Yao, X., Shu, J. (2025). Monitoring diurnal variations and displacement of surface urban heat islands using 10–minute himawari-8 data for urban climate adaptation. *Sustainable Cities and Society*, *130*, 106586. https://doi.org/10.1016/J.SCS.2025.106586

67. Wu, Q., Huang, Y., Irga, P., Kumar, P., Li, W., Wei, W., Shon, H. K., Lei, C., Zhou, J. L. (2024). Synergistic control of urban heat island and urban pollution island effects using green infrastructure. *Journal of Environmental Management*, *370*, 122985. https://doi.org/10.1016/J.JENVMAN.2024.122985

68. Yuan, B., Li, X., Zhou, L., Bai, T., Hu, T., Huang, J., Liu, D., Li, Y., Guo, J. (2023). Global distinct variations of surface urban heat islands in inter- and intra-cities revealed by local climate zones and seamless daily land surface temperature data. *ISPRS Journal of Photogrammetry and Remote Sensing*, *204*, 1–14. https://doi.org/10.1016/J.ISPRSJPRS.2023.08.012